Performance Study of Separate Exhaust Innovative Turbofan Engine Configurations with the Control Mechanism of a Baseline Engine

Elyas Lekzian[1*], Reza Modanlou[2]

[1]Assistant Professor, Faculty of New Sciences and Technologies, Aerospace Department, Semnan University, Semnan, Iran, e.lekzian@semnan.ac.ir

[2] MSc student, Faculty of New Sciences and Technologies, Aerospace Department, Semnan University, Semnan, Iran

Abstract:

In the current paper, an aero-thermodynamic solver is employed to simulate the performance of innovative turbofan engine layouts. The main aim is to investigate the key parameters such as thrust, specific fuel consumption (SFC), and engine efficiency. The innovative engine configurations are integrated with a base engine referred to as engine type1. Engine type 2 is constructed by adding a secondary combustion chamber, while engine type 3 incorporates a secondary inner bypass. Engine type 4 benefits from a secondary chamber and an inner bypass duct simultaneously. Flat rate analysis shows that engine type 1 turbine inlet temperature can increase up to 1708.5 K under ISA+30 condition. Additionally, the cruise thrust of engine type 2 can be enhanced by up to 77% with the penalty of 20% increase in SFC. An optimum reference inner bypass ratio is achieved for engine type 3, which simultaneously maximizes thrust and minimizes SFC. For Engine type 4, when sum of reference inner and outer bypass ratios equals 5.1, and the combustion chamber temperature matches that of baseline engine, it produces 17% higher cruise thrust than engine type 1. Besides, engine type 4 has higher cruise thrust at M=0.8 among all engine types. Engine type 2 and type 4 have higher flat rate performance (ISA+40). Engine type 3 has the highest overall efficiency, while engine type 2 demonstrates the lowest efficiency.

Keywords:

Aero-thermodynamic Solver, Second Bypass, Secondary Combustion Chamber, Performance, Flat rate.

1. Introduction

Modified aircraft layouts have become an attractive and ongoing field of study in recent years [1-3]. These aircrafts can use innovative turbofan engine configurations, which are designed to achieve lower fuel consumption, reduced No_x emissions, and decreased noise levels compared to conventional turbofan engines [4]. In general, the gas turbine combined cycles can even be utilized in stationary power generation powerhouses specially for reduction of No_x and other emissions [5, 6]. Additionally, in the aviation sector, the aim is to reduce fuel consumption and consequently reduce CO_2 as a pollutant [7].Due to these superiorities, continuous efforts are conducted to enhance the bypass of engine, leading to the concept of innovative engine layouts namely the ultra-high bypass engines [8, 9]. These engines exhibit lower SFC, but they also have drawbacks such as increased weight and higher nacelle drag due to their larger engine frontal aera [10]. Another innovative engine configuration which does not impose aforementioned high weight penalty of high bypass turbofan engines is the engine with a dual combustion chamber. These engines generate greater thrust or power but at the cost of increased fuel consumption [11]. The ultimate objective of this paper is to propose a combined engine configuration that leverages the advantages and mitigates the disadvantages of both aforementioned engine layouts. The novelty of this paper lies in the parametric study of adding a second bypass and a second chamber. In another word, current study aims to identify their optimal combinations for achieving optimized thrust and SFC. Therefore, it is worthwhile to address recent literature conducted on these two engine variants.

Lekzian et al. [12] studied a double bypass duct turbofan engine. Their Simulation results show that the double bypass duct engine produces 5.4% thrust more than the simple engine at M = 0.8 and at altitude of 9296.4 m. Additionally, they mentioned that the thrust of double bypass duct engine is more than the simple engine at SL altitude and at 9296.4 m at off-design conditions in all flight Mach numbers ranging from 0 to 0.8. Liu et al. [13] conducted a numerical investigation of a dual bypass compression system. They demonstrated that the operation of the system with a double bypass duct would lead to a broader fan operating range. Agulnik et al. [14] investigated a double bypass duct mixed exhaust turbofan engine. The second duct in their engine is adjustable. They proved that 7% SFC reduction can occur by

using the second bypass duct in subsonic flight regime. Manoharan [15] studied a separate exhaust two bypass duct turbofan engine using numerical propulsion simulation system software(NPSS). He concluded that his double bypass engine is more fuel efficient than the conventional one-bypass stream engine. Song et al. [16] simulated a two-bypass stream mixed exhaust turbofan engine. They analyzed the core stream fan inlet guide vane on the thrust, power and fuel consumption of engine at different second bypass ratios. Chen et al. [17] simulated a dual bypass mixed exhaust engine. They showed that engine thrust increases by up to 16% while SFC decreases by 1.2% under specific flight conditions. Aygun et al. [18] studied a variable cycle engine (VCE) that can operate in both single-bypass and double-bypass mode. They revealed that the SFC varies between 19.97 g/kN-s and 28.25 g/kN-s for VCE and between 23.91 g/kN-s and 31.14 g/kN-s for double-bypass mode.

In the field of engines with a second combustion chamber, as an relatively early study, Liew et al. [19] studied a separate exhaust turbofan engine. In their research, the secondary chamber was located after the high-pressure turbine. Their main outcome was that using a secondary chamber resulted in higher specific thrust. Furthermore, their results show that the specific fuel consumption is comparable to that of the base engine without a secondary chamber. The secondary chamber usually named as an interstage turbine burner (ITB) is also studied by Yin et al. [20]. Their research demonstrated that using an ITB could reduce NOx emissions by lowering the turbine inlet temperature (TIT) by approximately 300K. Pellgerini et al. [21] placed a second burner after the first turbine stage of a single-spool turbojet. They defined parameter called turbine split work (TWS), which represents the ratio of first stage turbine work to overall turbine work. They deduced that by using the secondary chamber, off-design TWS decreased by 30% compared to the design point. Kayadelan et al. [11] studied the addition of a second chamber after the high pressure turbine in a gas turbine cycle. They mentioned that net-work increased by reheating the flow after high pressure turbine by using the second chamber but SFC also increased. Levy et al. [22] studied a turbofan engine with ITB. The primary combustor of their engine used H_2 fuel, while the secondary combustor utilized hydrocarbon (jet or bio-jet) fuel. They reported that such configuration would lead to CO emission reduction.

Inspired from all the literature reviewed above, in the present study, a baseline well-known engine is considered. Then, an engine with secondary combustion chamber is studied. Effect of secondary

chamber temperature at the design and off-design point operation is investigated. Engine with secondary bypass is investigated in the next section of paper. This engine is also derived from the baseline engine. Additionally, a turbofan engine which simultaneously uses a secondary chamber and secondary bypass stream, is studied. The main aim of this paper is to study the effect of simultaneous addition of a bypass duct and a secondary chamber on the engine performance. Focus of the paper is mostly on the performance parameters including thrust, SFC, and overall efficiency. Moreover, the control mechanism of engine is identified and implemented on the engine for all the case-studies in this paper. The rest of this paper is organized as follows. The numerical aero-thermodynamic simulation methodology of engine is described. An in-house MATLAB code which is developed to study the engine configurations performance, is explained. In the next section, the accuracy of the developed methodology is verified by the available data of CFM56-7B engine. In the result section, the flat rate of engine is studied first. This section introduces a control mechanism for the engine. Then the performance of engine with interstage turbine burner (ITB) is studied. Effects of on-design and off-design ITB temperature at constant TIT on the cruise performance is studied. In the next section, engine performance with secondary bypass is investigated. Effect of second bypass ratio variation on the engine cruise performance is studied. Next part of paper is dedicated to the simulation of engine with simultaneous use of ITB and secondary bypass air stream. Then sea level and altitude performance of all engine types are compared.

2. Numerical Methodology

2-1- Aerothermodynamic Simulation

Aero-thermodynamic simulation is a fairly simple method utilized for engine performance study. This method satisfies conservation of mass, momentum, and energy for each component. The ratio of outlet/inlet total and static pressure (π) and temperature (τ) ratio for each component is considered as the thermodynamic simulation portion. The equations for losses in the intake and the Mach number at the exit nozzles are considered as the aerodynamic portion of the simulations. This method is widely and successfully used in many recent literatures to study gas turbine engine cycles [15-17]. In this paper,

for analysis of gas turbine on-design and off-design behavior, aero-thermodynamic simulation is utilized. Main inputs and outputs of the simulation are listed in Table 1.

Table 1 main inputs and outputs of engine simulation solver

				Design point	Off-Design Point
	Parameter	**unit**	**Description**	**Input/Output**	**Input/Output**
1	M_0	Dimeless.	Inlet Mach	Input	Input
2	h	m	Flight altitude	Input	Input
2	T_{t4}	K	HPT entry temperature	Input	Input
2	T_{t4d}	K	Second chamber exit temperature	Input	Input
3	$\dot{m}_0$	kg/s	Inlet mass flow rate	Input	Output
4	α_1, α_2	Dimless.	Bypass ratios	Input	Output
5	$\pi_{fan}, \pi_{LPC}, \pi_{HPC}$	Dimless.	Fan, LPC, HPC pressure ratio	Input	Output
6	F	kN or lbf	Thrust	Output	Output
7	SFC	lbm/lbf-hr	Specific fuel consumption	Output	Output
8	η_o	Dimless.	Overall efficiency	Output	Output

In the on-design simulation, the main design parameters include the flight Mach number, altitude of flight, first and second chamber outlet temperatures (which relate to the technology level of the turbine), and mass flow rate (which implies the weight and inlet frontal cross-section of the engine). Other parameters include the first and second bypass ratios (which imply the inner to outer duct area ratios), and the fan, LPC, and HPC compressor pressure ratios (which pertain to the compressor design issues). All these parameters must be set as design parameters, and then the thrust, SFC, and overall efficiency of the engine are obtained at on-design. The designed engine then experiences off-design conditions, including different Mach numbers and flight altitudes. Thus, these parameters are considered as inputs for the off-design simulations. Moreover, the first and second combustion chamber outlet temperatures can be adjusted by the fuel flow rate of the engine, which is actually adjusted by the throttle setting implemented by the pilot. The frontal area of the engine is fixed, and its dimensions have been determined in the design phase of the engine. Thus, the mass flow rate is obtained as a simulation result in the off-design phase. Since the outer to inner area ratio of the bypass duct is fixed in this paper, the outer and inner bypass ratios are also obtained from simulations at off-design conditions. The fan and

compressor pressure ratios are determined from the simulation results since the compressors and fans are designed at the on-design phase.

2-2- Fundamental Equations

The derivation of engine equations is very lengthy and equations are mainly attained by conservation of mass, momentum and energy. One of the key equations is the low-pressure turbine total temperature ratio (τ_{tL}) which results from energy balance between low-pressure turbine and low-pressure compressor-fan which are on the same spool. The final form of equation is as follows:

$$\tau_{tL} = 1 - \frac{\alpha_1 \tau_f \tau_d \tau_r + (\alpha_1 + \alpha_2 + 1)\tau_d \tau_r + (\alpha_2 + 1)\tau_f \tau_{cL} \tau_d \tau_r + (\alpha_1 + \alpha_2 + 1)\dfrac{C_{TO}}{\eta_{mP}}}{\eta_{mL}\left[\tau_{\lambda 2}\left\{\left[(1-\beta-\varepsilon_1-\varepsilon_2)(1+f\ )+\varepsilon_1\right](1+f_2)\right\}+\varepsilon_2 \tau_{cH} \tau_{cL} \tau_f \tau_d \tau_r\right]} \tag{1}$$

Where $\tau_{\lambda 2}$ is the second combustion chamber dimensionless temperature and is calculated as follows $\tau_{\lambda 2} = C_{pt} T_{t4d} / C_{pc} T_0$. Inner ($\alpha_2$) and outer ($\alpha_1$) bypass ratios at off-design are achieved by referencing their values with their corresponding design values. The final form of inner and outer bypass ratios are as follows:

$$\alpha_1 = \alpha_{1,R} \frac{\pi_{cH,R}\pi_{cL,R}}{\pi_{cH}\pi_{cL}} \sqrt{\frac{(\tau_{\lambda 1}/\tau_r \tau_d \tau_f)}{(\tau_{\lambda 1}/\tau_r \tau_d \tau_f)_R}} \frac{M_{9''}}{M_{9''_R}} \left[\frac{1+\left(\frac{\gamma-1}{2} M_{9''_R}{}^2\right)}{1+\left(\frac{\gamma-1}{2} M_{9''}{}^2\right)}\right]^{\left[\frac{\gamma+1}{2(\gamma-1)}\right]} \tag{2}$$

$$\alpha_2 = \alpha_{2,R} \frac{\pi_{cH,R}}{\pi_{cH}} \sqrt{\frac{(\tau_{\lambda 1}/\tau_r \tau_d \tau_f \tau_{cL})}{(\tau_{\lambda 1}/\tau_r \tau_d \tau_f \tau_{cL})_R}} \frac{M_{9'}}{M_{9'_R}} \left[\frac{1+\left(\frac{\gamma-1}{2} M_{9'_R}{}^2\right)}{1+\left(\frac{\gamma-1}{2} M_{9'}{}^2\right)}\right]^{\left[\frac{\gamma+1}{2(\gamma-1)}\right]} \tag{3}$$

The secondary chamber air fuel ratio (f_2) is a function of first and second combustion chamber outlet temperature. It is calculated as follows:

$$f_2 = \frac{\tau_{\lambda 2} - \tau_{tH}\tau_{m1}\tau_{\lambda 1}}{\dfrac{\eta_{b2} h_{PR}}{C_{pc} T_0} - \tau_{\lambda 2}} \tag{4}$$

Off-design fan total temperature ratio (τ_f) is attained using referencing method as follows:

$$\tau_f = A\left\{\tau_{f,R}\frac{1+\alpha_{1,R}+\alpha_{2,R}\tau_{cL,R}}{1+\alpha_1+\alpha_2\tau_{cL}}\right\}-A\left(\frac{1+\alpha_{1,R}+\alpha_{2,R}\tau_{cL,R}}{1+\alpha_1+\alpha_2\tau_{cL}}\right)\left(1-\frac{C_{TO,R}}{\eta_{mP}\tau_{d,R}\tau_{r,R}}\right)+\left(\frac{1+\alpha_1+\alpha_2}{1+\alpha_1+\alpha_2\tau_{cL}}\right)\left(1-\frac{C_{TO}}{\eta_{mP}\tau_d\tau_r}\right) \quad (5)$$

Where A is as follows:

$$A=\frac{\left(\tau_{\lambda 2}/\tau_r\right)}{\left(\tau_{\lambda 2,R}/\tau_{r,R}\right)}\frac{\tau_{d,R}}{\tau_d}\frac{\left(1-\tau_{tL}\right)}{\left(1-\tau_{tL,R}\right)} \quad (5\text{-}1)$$

2-3- Simulation Algorithm

For the performance simulation of engine, referencing method is used [23, 24]. In this method, the off-design parameters are achieved by using on-design values and also off-design input variables mentioned in preceding section. The general solution algorithm flowchart of engine is depicted in Figure 1. Main reference inputs are first and second chamber outlet on-design temperatures. Besides, the on-design values of inner and outer bypass ratios are considered as reference parameters. Other main inputs are off-design flight Mach number, flight altitude, and off-design combustion chambers outlet temperatures. The solution algorithm sets low pressure turbine pressure (π_{tL}) and temperature ratio (τ_{tL}), low pressure compressor temperature ratio (τ_{cL}), engine mass flow rate ($\dot{m}$), and fan temperature ratio (τ_f) as initial values. The pressure (π_{cH} , $\pi_{cL,}$) and temperature (τ_{cH} , τ_{cL}) of high and low pressure compressors are then calculated using referencing method. Next, the exit Mach numbers from core, inner, and outer bypass duct are calculated for converging exit nozzles of engine. Outer and inner bypass ratios are calculated based on equations (2) and (3). The value of π_{tL} and τ_{tL} are calculated sing equation (1). Off-design fan total temperature ratio (τ_f) is attained at next step using equation (5). In case that new value of τ_f is not equal to its previous value, its value decreased and calculations are repeated according to the block diagram from high pressure compressor (π_{cH} , τ_{cH}). Next step is -

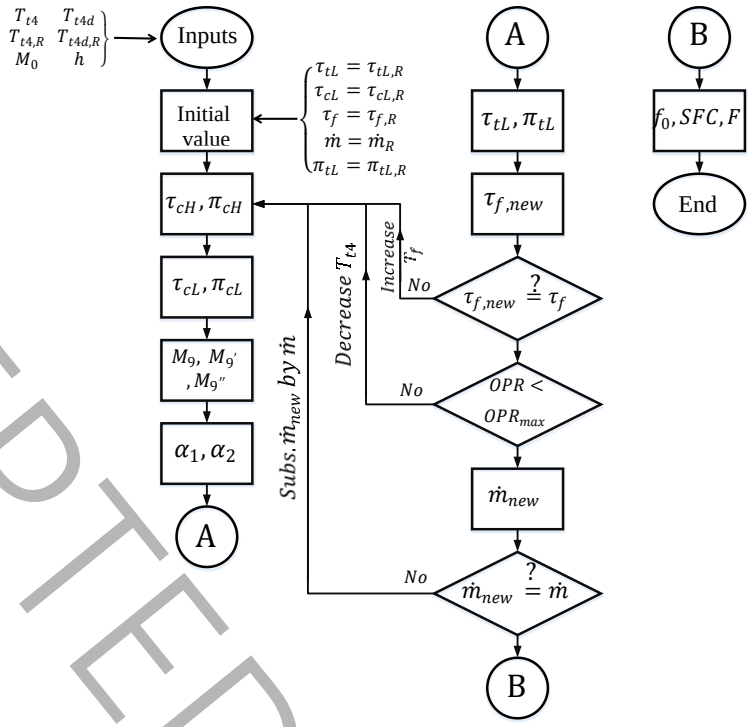

Figure 1 Flowchart of engine off-design simulation algorithm

checking the overall pressure of compressor. If it is more than maximum allowable value, the first chamber exit temperature decreased and calculations are repeated according to the block diagram from high pressure compressor (π_{cH} , τ_{cH}). This is the control mechanism of engine to prevent the engine from being overpressure and self-destruction. The mass flow rate is then calculated and its value compared with its previous value; If new value is not equal with its previous value, new mass flow rate is substituted by its old value and the calculations are repeated according to the block diagram from high pressure compressor (π_{cH} , τ_{cH}). At the end of off-design simulation, fuel flow (see equation (4)), thrust and SFC are calculated.

It is necessary to mention that the engine control mechanism relies on the engine theta break [25, 26] and the fact that the maximum simultaneous TIT and OPR are solely achieved at the theta break point.

3-Validation

CFM56-7B27 engine has one stage fan, three stages low-pressure compressor, nine stages high-pressure compressor, a can-annular combustion chamber, one stage high pressure turbine, and three stages low pressure turbine [27]. The validation of this engine is presented in the following section.

3-1-Main Performance Data

In this paper, typical component efficiencies, specific heats, combustion chamber and exhaust nozzle pressure losses are considered rationally by using the data suggested by Cihangir et al. [28]. Important engine data such as TIT, fan pressure ratio and compressor pressure ratio are adopted from reference [29, 30]. The reference point of engine is considered to be at sea level standard day condition at T.O. ($M_0 \approx 0$). Table 2 lists main performance parameters of the engine which are resulted from on-design and off-design performance calculations. Cruise to Take-off TIT ratio is a key performance parameter which is between 0.8 to 0.9 in thermodynamic analysis [20, 31, 32]. It is considered 0.87 in this study.

Table 2 Important on-design and off-design simulation Data

	Ref. [30]	**Current study**
Mass flow rate (kg/s) (cruise)	361	361
Mass flow rate (kg/s) (TO)	----	608
Cruise Thrust (lbf)	5480	5362
TO Thrust (kN)	121.5	121.4
BPR (cruise)	---	5.27
BPR (TO)	5.1	5.1
OPR	---	32.7

3-2-Shaft Speed

Corrected shaft speed is defined as follows:

$$CN_1 = \frac{N_1}{\sqrt{\theta_T}} \tag{6}$$

Where θ_T is the ratio of total temperature to the ambient temperature and calculated as follows:

$$\theta_T = \frac{T_t}{T_{amb}} \tag{7}$$

Also, the parameter N_1 is the low-pressure spool speed. It is obtained from the following equation:

$$N_1 = \sqrt{\frac{\left(\pi_f \pi_{cL}\right)^{\left[\frac{\gamma_c - 1}{\gamma_c}\right]}}{\left(\pi_{f,R} \pi_{cL,R}\right)^{\left[\frac{\gamma_c - 1}{\gamma_c}\right]}}} \tag{8}$$

The indices R in $\pi_{f,R}$ and $\pi_{cL,R}$ represent the on-design fan pressure ratio and low-pressure compressor pressure ratio, respectively. According to above mentioned equations, the generalized thrust curves can be established. The vertical axis in Figure 2 represents F/δ_{amb} (which is referred to as corrected thrust) and the horizontal axis represents the flight Mach number. The graph is plotted at different corrected speeds.

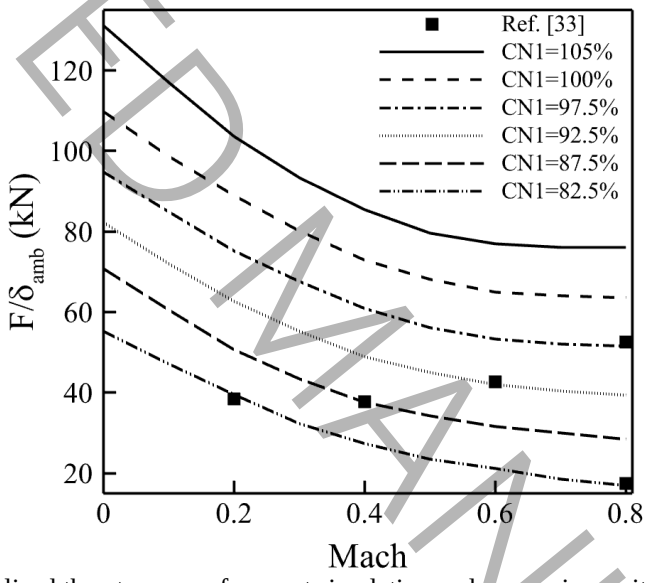

Figure 2 generalized thrust curves of current simulation and comparison with CFM56-7B27

Table 3 compares the simulation values with some of the corrected thrust values mentioned in reference [33]. It can be observed that maximum error is 3.1% which is fairly accurate regarding an aero-thermodynamic simulation for the engine [34].

Table 3 comparison of some of current corrected thrust values with reference data

$CN_1(\%)$	M_0	Current study	Reference [33]	Error (%)
		$\frac{F}{\delta_{amb}}$ (kN)	$\frac{F}{\delta_{amb}}$ (kN)	
82.5	0.2	39.545	38.433	2.9
82.5	0.8	16.903	17.437	3.1
87.5	0.4	37.498	37.72	0.5
92.5	0.6	41.946	42.614	1.6
97.5	0.8	51.599	52.622	1.9

3-3-Fuel Flow

Another aspect of verification study is the fuel flow. Fuel flow is equal to the specific fuel consumption multiplied by the engine thrust. It is common to plot the fuel flow in terms of corrected thrust at different Mach numbers. Therefore, the fuel flow versus corrected thrust is plotted at sea level and 10.67 km altitudes (Figure 3).

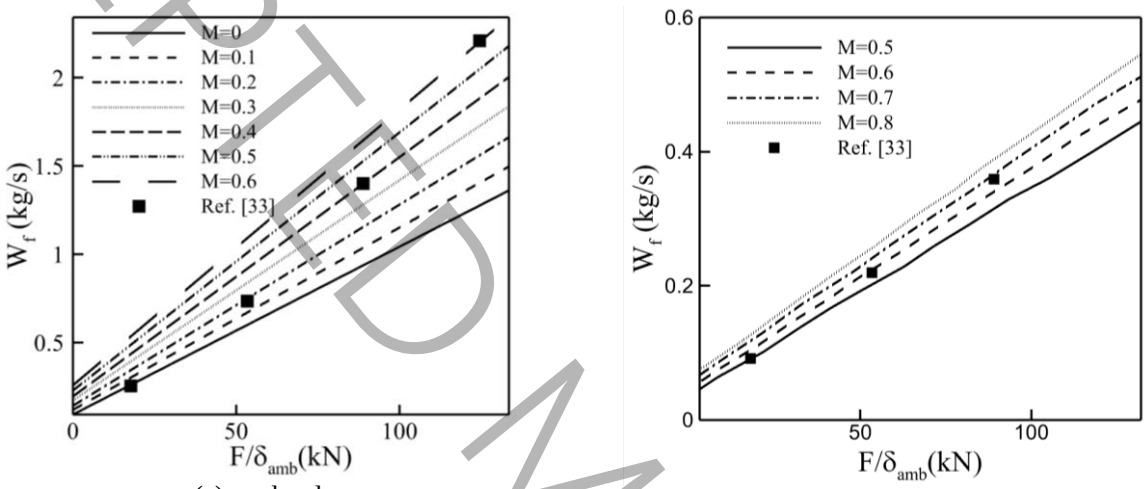

(a) sea level (b) 10.67 km

Figure 3 fuel flow variation at different Mach number

The results under different conditions are compared with some selected points of reference [33] and summarized in Table 4. It is seen that maximum error is 2.7% and once again it can be observed that results are in good agreement with the available real data.

Table 4 comparison of some of current fuel flow rate values with reference data

Altitude (ft)	Mach number	Corrected thrust F/δ_{amb} (kN)	Current study	Reference [33]	Error (%)
			W_f (kg/s)	W_f (kg/s)	
0	0	17.8	0.255	0.25	2.0
0	0.2	53.4	0.75	0.73	2.7
0	0.4	89	1.4	1.4	≈0
0	0.6	124.5	2.2	2.2	≈0
35000	0.5	17.8	0.092	0.094	2.1
35000	0.6	53.4	0.21	0.214	1.9
35000	0.7	89	0.35	0.36	2.7

4- Results and discussion

In this paper, four engine configurations are considered. All engines are twin spool and have separate exhaust ducts. Engine type 1 is similar to CFM56-7B27 which has a fan, LPC, HPC, combustion chamber, HPT, and LPT. Fan and LPT are on one spool, while the HPC and HPT are on the second spool. Engine type 2 is identical to engine type 1, but it also includes a secondary combustion chamber positioned between HPT and LPT. The secondary chamber allows for additional fuel-air mixing and combustion, and improving thrust but the efficiency and SFC must be studied. The term secondary chamber is mentioned as inter stage burner in many literatures [11, 35, 36]. Engine type 3 is derived from engine type 1, and its layout is the same as that of type 1, except that a secondary inner bypass duct is added to this engine. Also, HPC is extended up to the inner bypass duct. The reason for extension of HPC into inner bypass duct, is to increase the pressure into inner bypass more than simple engine. Engine type 4 has a second inner bypass duct, and a secondary chamber is also used in the engine core. The layouts of four engines are depicted in Figure 4 and their corresponding station numbers are listed in Table 5.

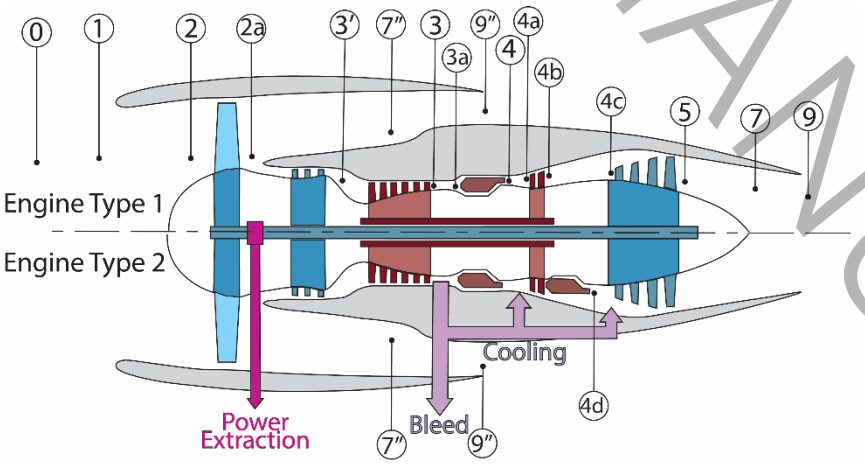

Table 5 engine stations numbering

Station	Description
0	Free stream
1	Inlet entry
2a	Fan exit
3'	LPC exit
3a	HPC exit
4	CC1 entry
4a	HPT entry
4b	HPT exit
4d	CC2 exit
4c	LPT entry
5	LPT exit
7	Core Exhaust Nozzle entry

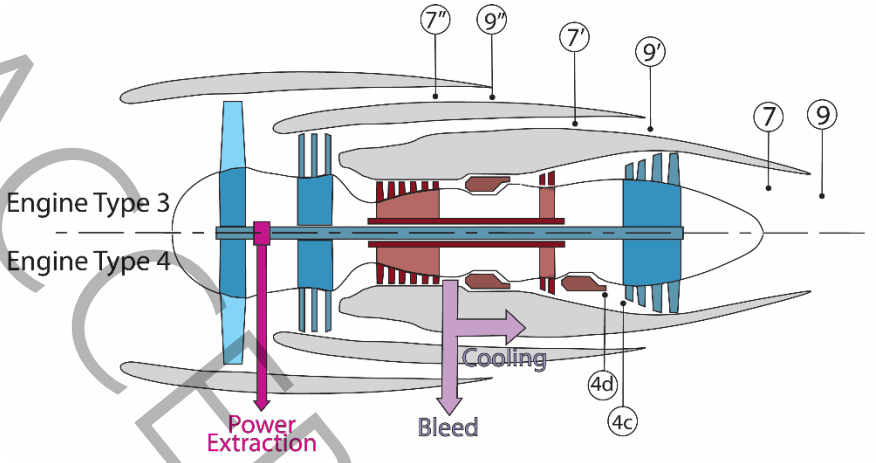

9	Core Exhaust nozzle exit
7''	Bypass 1 exhaust nozzle entry
9''	Bypass 1 exhaust nozzle exit
7'	Bypass 2 exhaust nozzle entry
9'	Bypass 2 exhaust nozzle exit

Figure 4 four types of engine layouts

In all engine types, first stage of both the high-pressure turbine and the low-pressure turbine are cooled. Besides, power is extracted from the low-pressure spool.

4-1-Flat Rate Analysis of Engine Type 1

The thrust produced by the engine is sensitive to changes in ambient air temperature. When the ambient temperature is low, the engine generates more thrust than necessary. At this condition, the engine thrust is flattened and controlled to not exceed a preset value. On the other hand, as the ambient temperature rises, the inlet air mass flow rate decreases, leading to reduced thrust. To maintain the desired thrust level, additional fuel must be injected, causing an increase in the turbine inlet temperature (TIT). Eventually, when the TIT reaches its maximum limit, thrust decreases as the ambient temperature continues to rise. This critical ambient temperature is referred to as the flat-rated temperature. Engine type 1 is considered as the benchmark case, and the performance parameters of other engine types are compared with this case. A flat rate analysis is performed for this engine to explore its control mechanism. It is assumed that ambient temperature is affected by ISA, but atmospheric pressure is only a function of altitude and remains fairly constant in the case of ISA variation. The flat rate analysis demonstrates that engine can generate thrust on a hot day as it can under ISA condition. According to reference [30], engine flat rate is 30 Celsius (303 K). At Sea level condition, engine TIT is 1624 K [29]. therefore, engine theta break (θ_{break}) is calculated as follows:

$$\theta_{break} = \frac{T_{t0}}{T_{std}} = \frac{303.15}{288.15} = 1.052 \quad (9)$$

As a result, the maximum allowable turbine inlet temperature at 303 K is calculated to be 1.052×1624=1708.5 K. By employing this control mechanism, engine type 1 flat rate is simulated and depicted in Figure 5. Figure 5 (a) shows that engine thrust is at its maximum at sea level static condition up to 303 K after which it decreases. In other words, flat-rated temperature is 303 K. At this condition the engine overall pressure ration (OPR) is maximum. Moreover, at partial throttle settings ($T_{t4}/T_{t4,max} = 0.95 \& 0.9$) the maximum OPR occurs at lower ambient temperatures. Between 253 to 303 K, the engine OPR is at its maximum, and above 303 K, turbine inlet temperature (TIT) is at its maximum. Both TIT and OPR reach their highest values at flat-rated temperature. Figure 5 (b) shows that engine TIT reaches its maximum at ambient temperatures (T_0) above 303 K. Besides, partial throttle settings show that flattened region of engine occurs in lower ambient temperature. Based on this control mechanism of engine explored here, The maximum allowable temperature of 1708.5 K is considered for all engine types in the rest of paper.

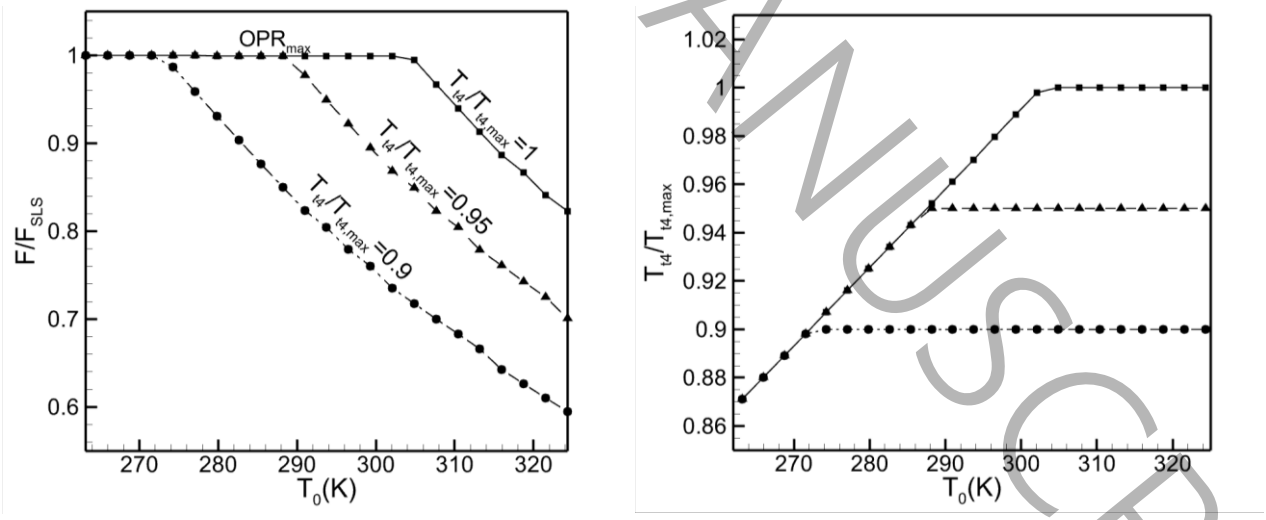

(a) thrust versus T_0

(b) T_{t4} versus T_0

Figure 5 engine flat rate

4-2-Performance Analysis of Engine Type 2

4-2-1-Parametric Study on T_{t4d} Variation

At this section, engine type 2 design-point TIT ($T_{t\,4,R} = 1624.5\ \mathrm{K}$) remains constant and is the same as that of engine type 1. Therefore, no technology level promotion for HPT blades is required. It is observed that thrust is increased linearly by elevating the off-design second chamber temperature ($T_{t\,4d}$). (Figure 6 (a)). The key finding is that highest engine thrust is obtained for the case in which $T_{t\,4d,R}$ is the same as engine type 1 ($T_{t\,4d,R} = 1260\ \mathrm{K}$), and off-design second chamber temperature ($T_{t\,4d}$) is 1778 K. At this condition, the thrust of engine type 2 increases by approximately 77% compared to engine -

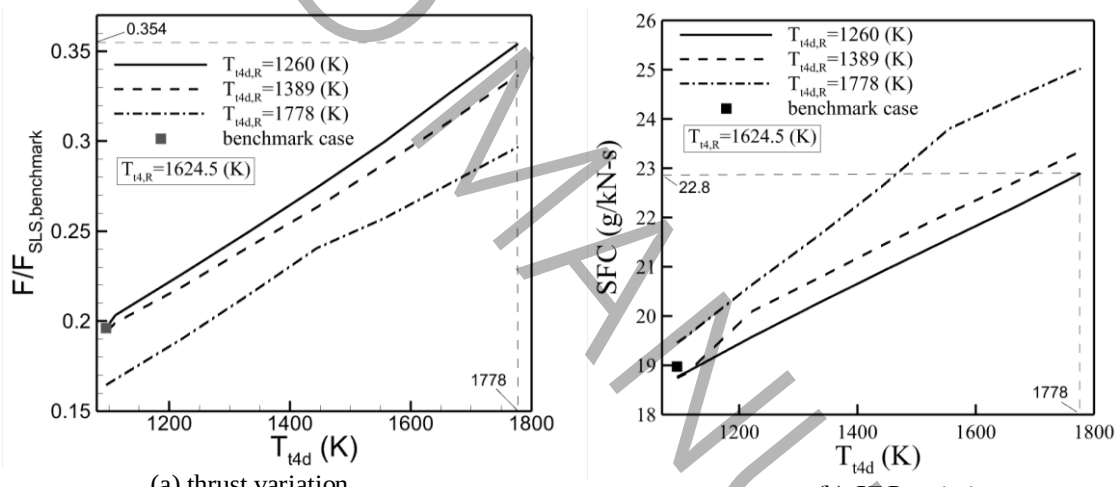

(a) thrust variation (b) SFC variation

Figure 6 thrust and SFC variation (engine type 2)

type 1, while SFC rises by up to 20 % (as shown in Figure 6 (b)). Consequently, it becomes reasonable to accept an SFC penalty to attain more thrust. The kinks observed in the graphs is due to the fact that the engine reaches to its maximum overall pressure ratio (32.9), leading to a decrease in $T_{t\,4}$ is decreased to control the engine pressure ratio.

4-2-2-Selected Cycle Performance for Engine Type 2

In this section, the point where both engines (engine type 1 and engine type 2) have the same cruise SFC, are selected. The aim at this section is to evaluate the thrust of engine type 2 in comparison with engine type 1, when the both engine types have the same SFC. The engines conditions at sea level and M=0 is considered exactly the same. Specifically, $T_{t4d,R}$ (i.e. T_{t4d} at h=SL and M=0) is selected to be 1260 K. It is observed that, engine type 2 thrust at h=10.67 km and M=0.8 is 7% more than benchmark engine (Table 6). Thus, this engine type can produce more thrust than engine type 1 while both using the sme cruise SFC. Another important issue is that in engine type 2, the first chamber temperature (T_{t4}) at cruise condition (h=10.67 km and M=0.8) is decreased to 1376 K. Additionally, engine type 2 overall efficiency is 3% less than engine type 1.

Table 6-performance parameters of engine type 1 and 2

	h=SL, M=0 (Reference condition)		**h=10.67 km, M=0.8**	
	Engine Type 1	**Engine Type 2**	**Engine Type 1**	**Engine Type 2**
T_{t4} (K)	1624	1624	1413	1376
T_{t4d} (K)	----	1260	----	1142
Thrust (kN)	121.5	121.1	23.8	25.5
SFC(g/kN-s)	11	11	19	19
η_o	----	----	0.3	0.29

4-3-Performance Analysis of Engine Type 3

4-3-1-Parametric Study on $\alpha_{2,R}/\alpha_{1,R}$ Variation

For analysis of engine type 3, sum of inner bypass $(\alpha_{2,R})$ and outer bypass $(\alpha_{1,R})$ is considered to be 5.1 $(\alpha_{1,R}+\alpha_{2,R}=5.1)$. The case where $\alpha_{2,R}=0$ is the base engine (engine type 1). Main aim is to increase the thrust and decrease the SFC in comparison with engine type 1 at cruise condition without excessive weight penalty due to fan diameter increase. Figure 7 shows variation of SFC (top figure) and thrust (middle figure) with on-design outer bypass ratio. Oscillation of data is due to the control mechanism of the engine. For better explanation of this oscillation, regarding Figure 7 (bottom figure) the engine reaches to the maximum OPR, therefore T_{t4} is decreased, SFC is increased and thrust is also decreased. By curve fitting the results, it is observed that an optimum design outer bypass ratio

corresponding to minimum SFC, occurs at $\alpha_{1,R} \approx 4.2$. Engine thrust at this condition is 25.2 kN. Under these circumstances, SFC is 3% less than engine type 1, and thrust is 6% more than the benchmark case.

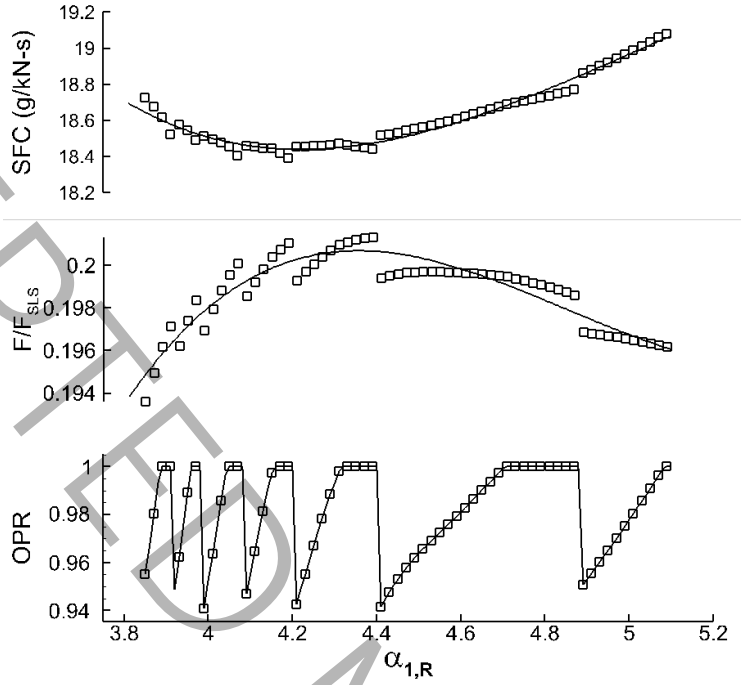

Figure 7 off-design SFC, thrust, and OPR variation with $\alpha_{1,R}$ (engine type 3)

Another, interesting issue can be obtained from Figure 7 is that higher on-design inner bypass ratios ($\alpha_{1,R}$), delays the point at which the engine reaches to its maximum OPR. The reason is that more fraction of thrust is provided by the bypass duct at this condition and the engine core contribution in thrust producing decreased. In another words, instead of achieving core engine compressor higher pressure ratios, thrust is attained by higher flow rate and pressure through the inner bypass duct.

4-3-2-Selected Cycle Performance for Engine Type 3

Utilizing the parametric study performed on engine type 3 in the preceding section, following performance is selected and shown in

Table 7. Thrust enhancement is 6% greater than the base engine (engine type 1), and SFC decreases by 3%. The overall efficiency of engine also increases by 3%.

Table 7-performance parameters of engine type 1 and type 3

	h=SL, M=0		h=10.67 km, M=0.8	
	Engine Type 1	**Engine Type 3**	**Engine Type 1**	**Engine Type 3**
T_{t4}(K)	1624	1624	1413	1413
α_1	5.1	4.2	5.43	4.14
α_2	0	0.9	0	0.96
Thrust (kN)	121.5	123	23.8	25.2
SFC(g/kN-s)	11	11	19	18.4
η_o	----	----	0.3	0.31

4-4-Performance Analysis of Engine Type 4

Engine type 4 benefits simultaneously from interstage burner and secondary bypass duct. Sea level performance of engine type 1 and type 4 is the same at M=0 (See Table 8). For engine type 4, $\alpha_{1,R}$ is considered 4.2 and $\alpha_{2,R}$ is equal to 0.9. Moreover, first chamber off-design outlet temperature is 1347 K and the second chamber off-design outlet temperature is 1206 K at 10.67 km (cruise condition). The pre-mentioned parameters are set in a way that cruise SFC (i.e. SFC at h=10.67 km and M=0.8) of the engine type 4 and type 1 be the same. For engine type 4, other parameters remain the same as baseline engine. Thrust, SFC, and overall efficiency of the engine is reported in Table 8.

Table 8-performance parameters of engine type 1 and 4

	h=SL, M=0		h=10.67km, M=0.8	
	Engine Type 1	**Engine Type 4**	**Engine Type 1**	**Engine Type 4**
α_1	5.1	4.2	5.43	4.42
α_2	0	0.9	0	0.98
T_{t4}(K)	1624	1624	1413	1347
T_{t4d} (K)	----	1260	----	1206
Thrust (kN)	121.5	123.2	23.8	27.9
SFC(g/kN-s)	11	11	19	19

η_o	----	----	0.3	0.3

Results show that thrust is increased 17% for this engine (engine type 4) in comparison with engine type 1. SFC is equal with the benchmark engine. An interesting finding is that first chamber temperature is 5% less than benchmark case. Therefore, high pressure turbine cooling considerations are decreased. Besides, low pressure turbine inlet temperature ($T_{t\,4d}$) is not higher than base engine and therefore no technology promotion for LPT is required. In other words, the design of engine type 4 is performed with minimum alterations compared to engine type 1, resulting in 17% thrust elevation at cruise conditions. Moreover, SFC and overall efficiency remains equal to the base engine.

4-5- T.O and Cruise Performance Comparisons of Four Engine Types

4-5-1-Sea Level Comparison: ISA Variation Effects on Engines T.O. Performance

Due to addition of second chamber and a second bypass, the temperature and pressure ratio of the fan and low-pressure turbine change. Consequently, the non-linear performance equations of engine are affected. Therefore, effect of ISA variation must be studied. The results show that addition of second bypass duct has no major effect on the engine flat rate in comparison with benchmark case. But as it can be seen in Figure 8, engine type 2 flat-rated temperature can vary by variation of $T_{t\,4d}$. It is observed that at $T_{t\,4d}\ /T_{t\,4,max} = 0.88$ the flat-rated temperature reaches to 313 K (40 ^{o}C). This implies that engine can operate at higher temperatures under sea level condition without thrust decay. One can conclude that addition of a secondary chamber is recommended for hot ISA+ conditions. The same behavior is observed for engine type 4.

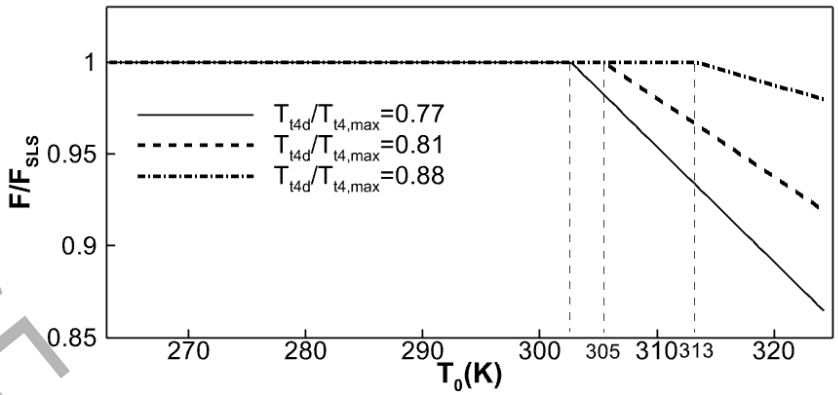

Figure 8 sea level flat rate operation (engine type 2 and type 4)

Figure 8 also illustrates that increasing the second chamber off-design outlet temperature $\left(T_{t\,4d}\ /T_{t\,4,max}\right)$ can heighten the flat-rated temperature but it should be noted that increasing $T_{t\,4d}$ is confined since the low-pressure turbine blade temperature withstanding limit.

4-5-2-Cruise Altitude Comparison

Figure 9 represents the thrust and SFC of four types engines at 10.67 km altitude. All engines exhibit higher thrust performance compared to the benchmark engine at all flight Mach numbers (Figure 9 (a)). Engine type 2 and type 4 have high fuel consumption across most flight Mach numbers (Figure 9 (b)). Engine type 3 shows the highest thrust performance at full throttle conditions during low cruise Mach numbers ranging from 0.4 to 0.7. This engine type has a sharp thrust decay rate, indicating its sensitivity to flight Mach number. However, it is important to note that this engine type exhibits lower fuel consumption in the Mach number range of 0.4 to 0.8 compared to other engine types. Engine type 4 exhibits thrust variation similar to type 2, but its thrust surpasses that of engine type 2 across all Mach numbers. Additionally, its fuel consumption at Mach=0.8 is equal with that of engine type 1.

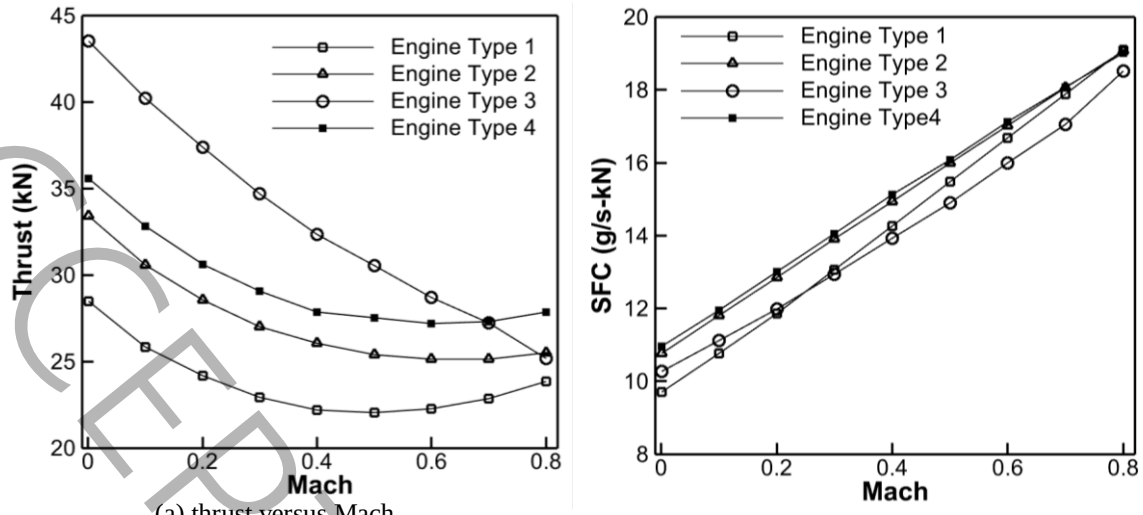

(a) thrust versus Mach (b) SFC versus Mach

Figure 9 Thrust and SFC at Alt.=10.67 km

It is observed that each engine type exhibits distinct performance characteristics, and selection of the engine depends on the specific mission objectives of the aircraft. If the engine is intended to operate within lower Mach numbers (between 0.4 to 0.7), engine type 3 is recommended. Conversely, for operations at higher Mach numbers, selecting engine type 4 is more rational.

5-Conclusion

In the current paper, an in-house MATLAB code was developed to simulate the performance of three innovative engine configurations. The main outcomes of this study are as follows:

1-The base engine (engine type 1) flat rate analysis shows that engine maximum operational TIT is 1708.5 K and the flat-rated temperature is 313 K. Below 313 K, the engine operates at maximum OPR, and over 313 K engine operates at maximum TIT.

2- Thrust for Engine Type 2 at Mach 0.8 and an altitude of 10.67 km (cruise condition) can increase by up to 77% compared to Engine Type 1 when the off-design secondary chamber outlet temperature (T_{t4d}) is equal to 1778 K. However, this improvement comes with a penalty of a 20% increase in specific fuel consumption (SFC).

3- In case that engine type 1 and type 2 have the same SFC, the thrust of engine type 2 is 7% more than that of engine type 1. Also, the off-design temperature at the outlet of the first chamber for engine type 2 ($T_{t4} = 1376$ K) is lower than benchmark case ($T_{t4} = 1413$ K) at cruise condition. Consequently, the

cooling requirements for the high-pressure turbine are less critical, leading to an increased life cycle for the high-pressure turbine blades in engine type 2.

4- Engine type 3 has an optimum reference inner bypass ratio which minimizes SFC of the engine at $\alpha_{1,R} = 4.2$. At this condition, thrust increases by 6% and the SFC decreases by 3% during cruise conditions compared to engine type 1.

6- The engine type 4 can produce 17% more cruise thrust than engine type 1 when $\alpha_{1,R} + \alpha_{2,R} = 5.1$, $T_{t\,4,R} = 1624K$ and $T_{t\,4d,R} = 1260$.

7- Results show that the flat-rated temperature for engine type 2 and type 4 can increase to 313 K by setting $T_{t\,4d} / T_{t\,4d,max} = 0.88$.

8- Engine type 3 exhibits higher cruise thrust value at low Mach numbers, ranging from 0.4 to 0.7. Additionally, it also, has lower specific fuel consumption during cruise. On the other hand, the engine type 4 produces higher thrust at high subsonic Mach numbers (*M*=0.7 to 0.8).

As future work, the design can be continued and modified using commercial software such as GT-Suite or AMESim to study and develop the control system in more detail, including the investigation of NO_x emissions and the modification of reheating cycles.

6- Nomenclature

C_{TO}	Dimensionless power off take
C_p, C_v	Heat capacity (J/kg-K)
h	Altitude (m)
F	Thrust (N)
f, f_0	Fuel air ratio/overall fuel air ratio
M	Mach number
h_{PR}	Fuel heating value (KJ/Kg)
m	Mass flow rate (kg/s)
P	Pressure (kPa)
T	Temperature (K)
R	Gas constant (J / Kg K)
SFC	Special fuel consumption (1/h)
$T_{t\,4}$ or TIT	First combustion chamber Temperature(K)
LPC,HPC	Low,High pressure compressor
$T_{t\,4d}$	Secondary chamber temperature (K)

Greek symbols

α	Bypass ratio
α_1, α_2	outer/inner bypass ratio
β	Bleed air fraction
γ	Heat capacity ratio
τ	Total temperature ratio
$\mathcal{E}$	Cooling air fraction
τ_λ	Stagnation enthalpy ratio of combustion chamber to free
π	Total Pressure ratio
η	efficiency

Subscript

b1, b2	First and second combustion chamber
r	Free stream
d	Diffuser (Intake)
f, cL, cH	Fan, low press. Compressor, high press.
tH, tL	High pressure turbine, low pressure turbine
1 to 9	Engine station number
R	Design point

7-References

[1] S. Hosseini, M.A. Vaziry-Zanjany, H.R. Ovesy, E. Lekzian, Multi-Objective Multidisciplinary Design Optimization of Regional Truss-Braced Wing Jet Aircraft, in: Aerospace Europe Conference 2023, 2023.

[2] P.-J. Proesmans, R. Vos, Airplane design optimization for minimal global warming impact, Journal of Aircraft, 59(5) (2022) 1363-1381.

[3] S. Karpuk, R. Radespiel, A. Elham, Assessment of future airframe and propulsion technologies on sustainability of next-generation mid-range aircraft, Aerospace, 9(5) (2022) 279.

[4] X. Xin, G. Huang, W. Lu, J. Wang, High bypass ratio turbofan engine with additional tip-driving fan: a design innovation, in: 51st AIAA/SAE/ASEE Joint Propulsion Conference, 2015, pp. 4022.

[5] F. Yin, A.G. Rao, A review of gas turbine engine with inter-stage turbine burner, Progress in Aerospace Sciences, 121 (2020) 100695.

[6] V. McDonell, M. Klein, Ground-based gas turbine combustion: metrics, constraints, and system interactions, Gas Turbine Emissions, 38 (2013) 24.

[7] A.J.A. Mom, 1 - Introduction to gas turbines, in: P. Jansohn (Ed.) Modern Gas Turbine Systems, Woodhead Publishing, 2013, pp. 3-20.

[8] T. Nikolaidis, S. Jafari, D. Bosak, P. Pilidis, Exchange rate analysis for ultra high bypass ratio geared turbofan engines, Applied Sciences, 10(21) (2020) 7945.

[9] A. Magrini, D. Buosi, E. Benini, Analysis of installation aerodynamics and comparison of optimised configuration of an ultra-high bypass ratio turbofan nacelle, Aerospace Science and Technology, 128 (2022) 107756.

[10] A. Magrini, E. Benini, H.-D. Yao, J. Postma, C. Sheaf, A review of installation effects of ultra-high bypass ratio engines, Progress in Aerospace Sciences, 119 (2020) 100680.

[11] H.K. Kayadelen, Y. Ust, V. Bashan, Thermodynamic performance analysis of state of the art gas turbine cycles with inter-stage turbine reheat and steam injection, Energy, 222 (2021) 119981.

[12] E. Lekzian, H. Farshi Fasih, R. Modanlou, Aerothermodynamic off-design performance study of a fixed double bypass duct turbofan engine, The Journal of Engine Research, 70(3) (2023) 62-75.

[13] B. Liu, R. Wang, X. Yu, On the mode transition of a double bypass variable cycle compression system, Aerospace Science and Technology, 98 (2020) 105743.

[14] A. Agul'nik, I. Kravchenko, A. Gorbunov, A. Novoselova, A. Sklyarova, Influence analysis of the second bypass air bleed parameters on the engine performance, Russian Aeronautics, 61 (2018) 441-444.

[15] S. Manoharan, Innovative Double Bypass Engine for Increased Performance, Embry-Riddle Aeronautical University, 2011.

[16] S. Fu, Z. Li, W. Zhanxue, L. Zhifu, S. Jingwei, Integration of high-fidelity model of forward variable area bypass injector into zero-dimensional variable cycle engine model, Chinese Journal of Aeronautics, 34(8) (2021) 1-15.

[17] H. Chen, Q. Zheng, Y. Gao, H. Zhang, Performance seeking control of minimum infrared characteristic on double bypass variable cycle engine, Aerospace Science and Technology, 108 (2021) 106359.

[18] H. Aygun, O. Turan, Exergetic sustainability off-design analysis of variable-cycle aero-engine in various bypass modes, Energy, 195 (2020) 117008.

[19] K.H. Liew, E. Urip, S.L. Yang, Parametric Cycle Analysis of a Turbofan Engine with an Interstage Turbine Burner, Journal of Propulsion and Power, 21(3) (2005) 546-551.

[20] F. Yin, A.G. Rao, Off-design performance of an interstage turbine burner turbofan engine, Journal of Engineering for Gas Turbines and Power, 139(8) (2017) 082603.

[21] A. Pellegrini, T. Nikolaidis, V. Pachidis, S. Köhler, On the performance simulation of inter-stage turbine reheat, Applied Thermal Engineering, 113 (2017) 544-553.

[22] Y. Levy, V. Erenburg, V. Sherbaum, I. Gaissinski, Development of combustor for a hybrid turbofan engine, International Journal of Turbo & Jet-Engines, 39(4) (2022) 465-475.

[23] J.D. Mattingly, W.H. Heiser, D.T. Pratt, Aircraft Engine Design, 2nd ed., American Institute of Aeronautics & Astronautics, Reston, Virginias, 2002.

[24] S. Farokhi, Aircraft Propulsion, 2nd ed., Wiley, Kansas, USA, 2009.

[25] D. Levin, D. Parsons, D. Panteny, P. Wilson, M. Rask, F-35 STOVL Performance Requirements Verification, in: 2018 Aviation Technology, Integration, and Operations Conference.

[26] R.A. Clark, J. Tai, D. Mavris, Integrated Design of a Variable Cycle Engine and Aircraft Thermal Management System, in: Turbo Expo: Power for Land, Sea, and Air, American Society of Mechanical Engineers, 2023, pp. V001T001A036.

[27] O. Turan, Exergo-economic analysis of a CFM56-7B turbofan engine, Energy, 259 (2022) 124936.

[28] S.A. Cihangir, H. Aygun, O. Turan, Energy and performance analysis of a turbofan engine with the aid of dynamic component efficiencies, Energy, 260 (2022) 125085.

[29] H. Aydin, O. Turan, T.H. Karakoc, A. Midilli, Exergetic sustainability indicators as a tool in commercial aircraft: a case study for a turbofan engine, International journal of green energy, 12(1) (2015) 28-40.

[30] M. Daly, G. Bill, Jane's Aero Engines 2013/2014, Jane's Information Group, 2013.

[31] A. Ghenaiet, Analyses and Optimization of a Propulsion Cycle for Unmixed High Bypass Turbofan, in: Turbo Expo: Power for Land, Sea, and Air, 2008, pp. 473-488.

[32] D. Papamoschou, M. Debiasi, Conceptual development of quiet turbofan engines for supersonic aircraft, Journal of propulsion and power, 19(2) (2003) 161-169.

[33] Boeing, Boeing 737-800 Performance Engineers Manual, 1998.

[34] V. Sanghi, B. Lakshmanan, V. Sundararajan, Digital simulator for steady-state performance prediction of military turbofan engine, Journal of Propulsion and Power, 14(1) (1998) 74-81.

[35] Z. Ji, J. Qin, K. Cheng, H. Liu, S. Zhang, P. Dong, Performance evaluation of a turbojet engine integrated with interstage turbine burner and solid oxide fuel cell, Energy, 168 (2019) 702-711.

[36] T. Blondeel, F. Yin, A. Gangoli Rao, A Novel Engine Architecture for Low NOx Emissions, in: Turbo Expo: Power for Land, Sea, and Air, American Society of Mechanical Engineers, (2022), pp. 46-57.